ISSN 1054-660X, Laser Physics, 2012, Vol. 22, No. 12, pp. 1767–1770.

Filament-Induced Breakdown Remote Spectroscopy in a Polar Environment[1]

H. L. Xu[a, c, *], P. T. Simard[a], Y. Kamali[a], J.-F. Daigle[a], C. Marceau[a], J. Bernhardt[a], J. Dubois[b], M. Châteauneuf[b], F. Théberge[b], G. Roy[b], and S. L. Chin[a]

[a] *Centre d'Optique, Photonique et Laser et le Département de Physique, Université Laval, QC, G1V0A6, Canada*
[b] *Defense Research and Development Canada Valcartier, 2459Pie XI Blvd North, Québec, QC, G3J 1X5, Canada*
[c] *State Key Laboratory on Integrated Optoelectronics, College of Electronic Science and Engineering, Jilin University, Changchun 130012, China*

*e-mail: huailiang.xu@gmail.com

Received September 27, 2011; in final form, October 5, 2011

Abstract—We demonstrate the feasibility of filament-induced breakdown spectroscopy (FIBS) for remote sensing of solid samples in a polar environment. FIBS spectra from an aluminum target induced by 800-nm laser pulses propagating in air were probed. The air visibility in an open winter field was as low as 3.2 km fluctuating with precipitation, pressure and relative humidity. Under such polar condition, clean spectral Al I lines from an aluminum target located at a distance of 60 m were obtained. This shows the technique FIBS could be potentially useful for sensing remote targets in a variety of polar environments.

DOI: 10.1134/S1054660X12120298

1. INTRODUCTION

When a pulsed laser with sufficient high energy is tightly focused onto the surface of a sample, the material can rapidly reach its vaporization temperature and small amounts of target material are ablated into plasma that emits characteristic spectral lines or bands. The properties of the plasma and the material compounds can thus be determined based on the measured emission spectra. This technique, popularly called laser-induced breakdown spectroscopy (LIBS) or laser-induced plasma spectroscopy (LIPS), has been proved to be very powerful for rapid, on-line and multi-elemental material analysis without sample preparation [1–5].

LIBS using femtosecond laser pulses (fs-LIBS) has attracted much attention because of its promising properties including lower ablation energy threshold, low continuum emission, higher sensitivity and improved detection precision [6, 7]. In particular, a special configuration of fs-LIBS, called filament-induced breakdown spectroscopy (FIBS), was proposed for remote elemental analysis of metallic as well as biological samples [8, 9]. The FIBS scheme is based on the filamentation of non-linear propagation of femtosecond laser pulses in air [10–15]. When intense femtosecond laser pulses propagate in air, Kerr self-focusing occurs; it is then balanced by the defocusing of plasma generated by multi-photon/tunnel ionization of air molecules. Associated with filamentation, several interesting nonlinear phenomena such as strong THz emissions could occur [16–18]. The dynamical equilibrium in the filamentation process leads to an almost constant laser intensity inside the filament core (intensity clamping) [10–12, 19]. At 800 nm, in air, the laser intensity is about 5×10^{13} W/cm^2 [20–22]. This high intensity can fragment gas molecules and aerosols as well as induce breakdown on solid targets [23–25]. The intensity clamping inside filaments minimizes energy fluctuation and self-stabilizes the spatial mode quality in the interaction zone (filament zone) [26, 27]. The energy stabilization, as one of the factors that determine the sensitivity and stabilization of the FIBS signal, would help to improve remote sample detection [28]. Moreover, it was reported that filamentation could occur at a distance as long as a few kilometers in the atmosphere [29], overcoming the diffraction limit of conventional ns-LIBS to remotely deliver high laser intensity, which may suggest FIBS potentially useful for remote, contact-free process control and multi-elemental analysis in a kilometer range.

So far, apart from [8] and a brief introduction of the current subject in a recent review [30], the measurements concerning remote sensing of samples using FIBS have been performed mainly in the laboratory environments (see, e.g. [31] and references therein). The purpose of this study is aimed at demonstrating the capacity of this technique in outdoor polar environments. Since metallic surface characterization represents an interesting issue for real-time industrial metallurgic production analysis, we study in this paper the metallic aluminum target located in an open winter field using FIBS. Outdoor experiments at very low temperature (–20°C or below) in the winter is not trivial as one would normally imagine since the performance is limited by many factors that need to be over-

[1] The article is published in the original.

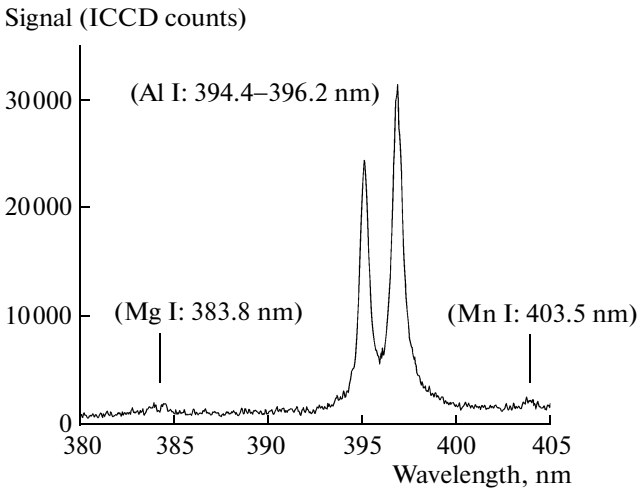

Fig. 1. Filament-induced spectra of aluminum recorded at a distance of 32 m in a winter field with an air visibility of ~14.4 km. The laser pulse energy was 225 mJ/pulse and the laser pulse duration was negatively chirped to 2 ps. The data were averaged over 10 laser shots.

come when compared with those experiments carried out in laboratories and also those outdoor experiments with a moderate temperature in the range of 10–30°C. In this experiment, the open air visibility was as low as 3.2 km which fluctuates with precipitations (snow), pressure and relative humidity. The laser beam had to go through a very large temperature gradient from the warm laser room to the open air. Even so, clean atomic Al I line signals were observed, showing potential applications of this technique, FIBS, in remote sensing of elements under adverse winter conditions.

2. EXPERIMENTS

The experiment was conducted using the T&T (Terawatt and Terahertz) laser system [32] at the Defense Research and Development Canada (DRDC) in Valcartier which delivered an energy of about 225 mJ per pulse. The pulse duration was about 45 fs and could be negatively chirped up to 8.5 ps. The wavelength of the laser pulses was centered at 800 nm and the repetition rate was 10 Hz. The compact laser system stood on a 1.25×2.5 m^2 table mounted in a container which could be brought into the open field. A sending telescopic system [33] was used to control the filament locations in the open area at a distance up to 60 meters available for this experiment in Valcartier. A LIDAR (LIght Detection And Ranging) collection system was built with a concave mirror which had a diameter of 28 cm and a focal length of $f = 150$ cm and with a fiber bundle that collected the signals. The sending telescope and LIDAR systems were both installed inside a garage whose door opened to a 60–80 m long field surrounded by a 5-m high sand bank. Everywhere outside the garage was covered by snow more than 1 m high. Therefore, a trail was mechanically shoveled out to accommodate the propagation of the laser beam so that the installation of the target at different distances could be much easier. The aluminum sample (ALCAN, a standard usage grade 6061) was fixed on a rotation stage which was driven by a step motor in order to give a fresh target surface for each laser shot.

The signals collected by the LIDAR system were then delivered to a spectrometer (Acton Research SpectraPro 500i) coupled to an ICCD (Intensified Charged Coupled Device) camera (Princeton Instrument PI-MAX). The spectral resolution was 0.4 nm [34]. Both the spectrometer and the ICCD were enclosed inside a heating system in order to prevent condensations in the winter season. The spectrometer was found to have a slight offset of about 0.5 nm according to the wavelength calibration made with a He–Ne laser at 632.3 nm.

3. RESULTS AND DISCUSSION

Using the FIBS technique, the aluminum sample was first probed in an outdoor environment at noon of a sunny day with the weather conditions monitored by the DRDC-Valcartier meteorological station. Three main weather parameters, i.e., visibility, temperature and the temperature gradient over the laser propagation axis were recorded. The visibility was defined using Runway Visual Range (RVR) airport measurement. The outside temperature was measured to be –20°C, and the dew point –22°C. The visibility was more than 14.4 km for the clear sunny day, and the pressure and relative humidity were measured to be 1.0025×10^5 Pa and 50%, respectively. The temperature inside the laser container was kept constant at 20°C with a measurement uncertainty of ±0.2°C. The heating system generated a hot air flow inside the garage. Between the garage and the outside field, an industrial heater was installed in a supplementary protective chamber made of wood. Hence, there existed a temperature gradient. This introduced a dynamic non-uniform air turbulence which constantly modified the laser spatial mode quality before the filaments were formed.

When the target was located at a distance of 32 m from the laser system and the industrial heater between the garage and the outside field was temporarily turned off to reduce the air turbulence, the signals from the $3s^2 4s$–$3s^2 3p$ transitions of Al I lines at 394.4 and 396.2 nm were clearly observed, as shown in Fig. 1. In this measurement, the laser pulse duration was negatively chirped to 2 ps and the laser energy was 225 mJ/pulse. The data were averaged over 10 laser shots. The ICCD gate width was set to 2 μs and the ICCD delay time was set to be 30 ns after receiving the laser light scattering from the target. The filament starting position was estimated by a burn paper to be

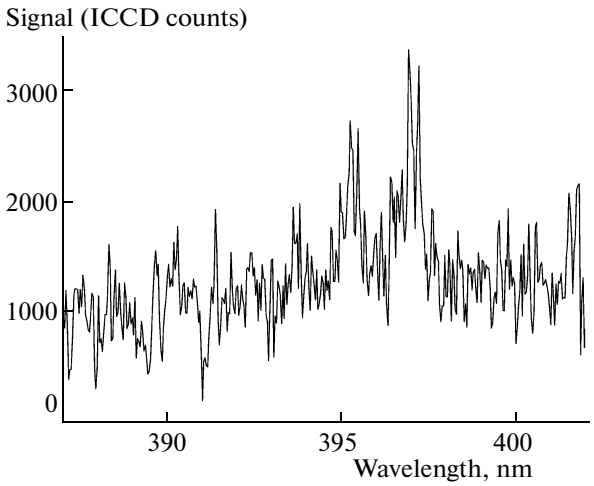

Fig. 2. Filament-induced spectrum of aluminum recorded at a distance of 60 m in a winter field with an air visibility of ~3.2 km.

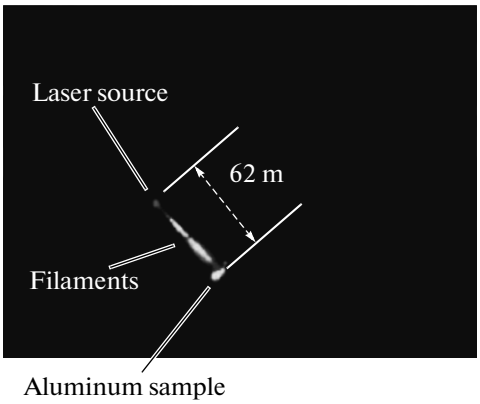

Fig. 3. Outdoor laser propagation picture taken with a digital camera. This picture was taken after sunset while snow fall was relatively dense. The bright light was from scattering of the laser and the generated white light by snowflakes.

roughly 1 m before the target which was measured through listening to the strong acoustic signal (sound) on a burn paper. In addition, the door was opened and the laser passed through a small hole on the protective chamber. The temperature gradient of about 40°C was kept within a distance of about 2-m long. It could be noticed in Fig. 1 that there are two weak peaks at 383.8 and 403.5 nm, which were assigned to Mg I and Mn I, resulting from the trace elements in the aluminum sample (Mg: 0.8–1.2 wt % and Mn: <0.15 wt %).

Next, we show the feasibility of the FIBS for detecting the aluminum sample at a distance of 60 m in the polar environment with a dense snow fall and a weak fog that lowered the air visibility down to 3.2 km. The temperature, dew point, pressure and relative humidity were −7, −12°C, 1.005×10^5 Pa and 68%, respectively. In this measurement, the industrial heater was turned off. The laser beam passed through the hole of the protective chamber. In this polar environment, the Al lines at 394.4 and 396.2 nm were still observed, as shown in Fig. 2. The ICCD gate width was set to 2 μs. The laser energy was 220 mJ/pulse and the pulse duration was negatively chirped to 8.5 ps in order to generate the filaments to a distance of 60 m. In this measurement, the ICCD gate delay was set to 480 ns after receiving the laser light scattering from the target. This value is not well set during the experiment, which may be optimized to give rise to an enhanced signal. Since there was a strict time limitation for using the laser system in a daytime in Valcartier, and it is thus difficult to arrange another experiments in the same weather condition, the experiments could not be repeated as those in the laboratory environment although the noise level is relatively large. It is expected that when the laser and filament conditions as well the detection system are optimized, the signal could be enhanced significantly. Figures 3 show the laser propagation picture taken with a digital camera with the sample at a distance of about 60–62 m from the garage door. The picture was taken after sunset while snow fall was relatively dense. As a consequence, the observed Al lines at 394.4 and 396.2 nm clearly show the potential of the FIBS technique in the application to remote sensing in a polar environment.

In order to get more insight into the application of FIBS technique, it will be helpful to estimate an optimum detection distance based on the data obtained in our experiment. Because of intensity clamping, we assume that the filament-induced FIBS signal is independent of the propagation distance of the laser pulse before the filament hits the sample. We use the spectrum in Fig. 1 as an example. The intensity of the strongest spectral line at 397 nm ($4s\,^2S_{1/2} \longrightarrow 3p\,^2P^{\circ}_{3/2}$)

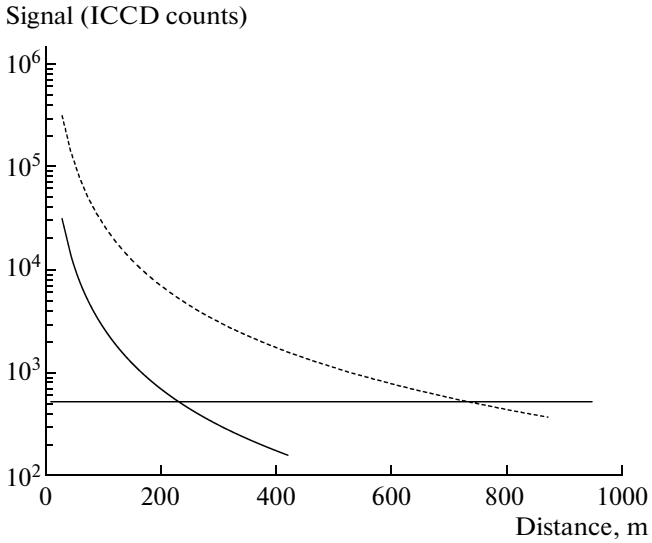

Fig. 4. Extrapolation of the 3σ detection limit.

in Fig. 1 is as high as 31370 ICCD counts. Therefore, from the LIDAR equation $I \propto 1/R^2$, where I is the signal intensity and R the distance between the sample and the detector [35], the detection limit of 3σ, as shown in Fig. 4, would reach to about 230 m (solid line); here σ is the standard deviation of the background noise level. There is a lot of room to improve our experiment in the future such as improving the laser beam quality using adaptive optics, enhancing the collection efficiency by replacing the ICCD by a PMT, using a larger telescope, etc., it is reasonable to expect that the signal could be enhanced at least by a factor of 10. Consequently, the detection limit of 3σ would be reached at a distance of about 730 m, as shown by the dash line in Fig. 4. That is to say, kilometer range of detection capability would be reachable even in an adverse polar environment.

4. CONCLUSIONS

In summary, using the FIBS technique, we experimentally demonstrate the plasma emission from an aluminum target in the atmosphere in an adverse environment with dense snow. With the developments of femtosecond laser techniques and new methods in controlling the location and numbers of laser multifilaments [36, 37], it would be possible in the future to extend the detection up to the kilometer range, which makes it promising for the remote detection of environmental contamination.

ACKNOWLEDGMENTS

We acknowledge the technical support of M. Martin, M. Jean, and M. Cardinal. This work was partially supported by NSERC, DRDC Valcartier, Canada Research Chairs, CIPI, CFI, Femtotech, and FQRNT.

REFERENCES

1. H. R. Griem, *Plasma Spectroscopy* (McGraw-Hill, 1964).
2. D. A. Cremers and L. J. Radziemski, *Handbook of Laser-Induced Breakdown Spectroscopy* (Wiley, 2006).
3. A. A. I. Khalil, M. Richardson, L. Johnson, and M. A. Gondal, Laser Phys. **19**, 1981 (2009).
4. E. L. Surmenko, T. N. Sokolova, Yu. V. Chebotarevsky, and I. A. Popov, Laser Phys. **19**, 1373 (2009).
5. A. A. I. Khalil, Laser Phys. **20**, 238 (2010).
6. V. Margetic, A. Pakulev, A. Stockhaus, et al., Spectrochim. Acta, Part B **55**, 1771 (2000).
7. K. L. Eland, D. N. Stratis, D. M. Gold, et ak,, Appl. Spectrosc. **55**, 286 (2001).
8. K. Stelmaszczyk, P. Rohwetter, G. Méjean, et al., Appl. Phys. Lett. **85**, 3977(2004).
9. H. L. Xu, W. Liu, and S. L. Chin, Opt. Lett. **31**, 1540 (2006).
10. S. L. Chin, S. A. Hosseini, W. Liu, et al., Can. J. Phys. **83**, 863 (2005).
11. A. Couairon and A. Mysyrowicz, Phys. Rep. **441**, 47 (2007).
12. L. Berge, S. Skupin, R. Nuter, et al., Rep. Prog. Phys. **70**, 1633 (2007).
13. J. Kasparian and J.-P. Wolf, Opt. Express **16**, 466 (2008).
14. V. P. Kandidov, S. A. Shlenov, and O. G. Kosareva, Quantum Electron. **39**, 205 (2009).
15. S. L. Chin, *Femtosecond Laser Filamentation* (Springer-Verlag, 2010).
16. T.-J. Wang, J.-F. Daigle, Y. Chen, et al., Laser Phys. Lett. **7**, 517 (2010).
17. T.-J. Wang, C. Marceau, S. Yuan, et al., Laser Phys. Lett. **8**, 57 (2011).
18. T.-J. Wang, S. Yuan, Z.-D. Sun, et al., Laser Phys. Lett. **8**, 295 (2011).
19. W. Liu, S. Petit, A. Becker, et al., Opt. Commun. **201**, 189 (2002).
20. A. Becker, N. Akózbek, K. Vijayalakshmi, et al., Appl. Phys., Ser. B **73**, 287 (2001).
21. J. Kasparian, R. Sauerbrey, and S. L. Chin, Appl. Phys., Ser. B **71**, 877 (2000).
22. Z. G. Ji, J. S. Liu, Z. X. Wang, et al., Laser Phys. **20**, 886 (2010).
23. H. L. Xu, Y. Kamali, C. Marceau, et al., Appl. Phys. Lett. **90**, 101106 (2007).
24. J.-F. Daigle, G. Méjean, W. Liu, et al., Appl. Phys., Ser. B **87**, 749 (2007).
25. H. L. Xu, J. Bernhardt, P. Mathieu, et al., J. Appl. Phys. **101**, 033124 (2007).
26. F. Théberge, N. Akózbek, W. Liu, et al., Phys. Rev. Lett. **97**, 023904 (2006).
27. W. Liu and S. L. Chin, Phys. Rev., Ser. A **76**, 013826 (2007).
28. S. Q. Xu, Y. Zhang, W. Liu, and S. L. Chin, Opt. Commum. **282**, 4800 (2009).
29. M. Rodriguez, R. Bourayou, G. Méjean, et al., Phys. Rev., Ser. E **69**, 036607 (2004).
30. S. L. Chin, H. L. Xu, Q. Luo, et al., Appl. Phys., Ser. B **95**, 1 (2009).
31. H. L. Xu and S. L. Chin, Sensors **11**, 32 (2011).
32. M. Cháteauneuf and J. Dubois, http://spie.org/x8496.xml?ArticleID=x8496.
33. W. Liu, F. Théberge, J. F. Daigle, et al., Appl. Phys., Ser. B **85**, 55 (2006).
34. Q. Luo, H. L. Xu, S. A. Hosseini, et al., Appl. Phys., Ser. B **82**, 105 (2006).
35. Q. Luo, J. Yu, S. A. Hosseini, et al., Appl. Opt. **44**, 391 (2005).
36. S. A. Hosseini, Q. Luo, B. Ferland, et al., Phys. Rev., Ser. A **70**, 033802 (2004).
37. S. Skupin, L. Bergé, U. Peschel, et al., Phys. Rev., Ser. E **70**, 046602 (2004).